Three-level Λ-type microwave memory via parametric-modulation-induced transparency in a superconducting quantum circuit

Kai-I Chu [1,2] Wen-Te Liao [2,3,4,5] and Yung-Fu Chen [2,5,*]

[1]*Molecular Science and Technology Program, Taiwan International Graduate Program, Academia Sinica, Taipei 11529, Taiwan*
[2]*Department of Physics, National Central University, Taoyuan City 32001, Taiwan*
[3]*Physics Division, National Center for Theoretical Sciences, Taipei 10617, Taiwan*
[4]*Center for Quantum Technology, Hsinchu 30013, Taiwan*
[5]*Quantum Technology Center, National Central University, Taoyuan City 32001, Taiwan*

(Received 22 May 2023; accepted 8 August 2023; published 18 September 2023; corrected 5 October 2023)

We investigate theoretically a type of microwave memory that is composed of a single transmon qubit and a coupling resonator. The synergy of the parametric modulation of the qubit resonance frequency and a microwave directly driving the qubit transition can constitute effective three-level Λ-type electromagnetically induced transparency. We demonstrate that the dynamical control of such a parametric modulation allows for the possibility of microwave storage and retrieval using a single qubit. Our results pave the way towards the practical implementation of quantum information in superconducting circuits.

DOI: 10.1103/PhysRevResearch.5.033192

I. INTRODUCTION

Optical quantum memory serves as a key ingredient for quantum information processing. Through this device, one can store and retrieve photonic information on demand for long-distance quantum communications and quantum computations [1,2]. In optical systems, the idea of quantum memory can be realized more easily due to the existence of many long-lived metastable states in natural atoms. Many light storage protocols, e.g., electromagnetically induced transparency (EIT), gradient echo, and atomic frequency combs, have been demonstrated over the past few decades [3–10]. Remarkably, a very high memory efficiency up to 92% based on a three-level Λ-type EIT system has been experimentally realized [11]. Electromagnetically induced transparency is a quantum interference effect making atoms transparent to a weak resonant probe field due to the existence of another strong-coupling field. In EIT media, a probe pulse slowly travels with a controllable group velocity, and can even stop in the media [12], because the dispersion of the probe light is greatly modified to become steep by the coupling field. The EIT optical memory is realized by adiabatically turning off the coupling light, which transfers the probe field's coherence to the atomic coherence [13].

As for the microwave regime, superconducting-circuit-based quantum computing research has developed substantially over the past few years [14,15]. It is therefore natural to search for an analogous microwave quantum memory to scale up to a larger quantum network [2] in the superconducting circuit community. One promising approach is to leverage high-quality resonators [16] for storing quantum information [17–21]. Previous studies have demonstrated microwave storage and retrieval by manipulating the coupling between the resonator and the information propagation channel [22–24]. However, the protocol is specifically suitable for exponentially rising pulses, the time-reversed pulses of radiative decay. More recently, researchers utilized arrays of resonators, resembling atomic frequency combs, to achieve broadband microwave storage [25,26]. The direct coupling between on-chip resonators might result in impedance mismatching, decreasing the memory efficiency [26].

Here we aim to realize a microwave memory based on EIT, allowing for the storage and preservation of arbitrary waveforms. However, realizing EIT in superconducting circuits is difficult because most of the superconducting atoms lack suitable metastable states. Some protocols use a single Ξ-type superconducting atom strongly coupling to an open transmission line [27,28]. Due to the short coherence time of the atom, the optical response is Autler-Townes splitting (ATS) rather than EIT [29]. Several groups recently worked on designing an effective Λ-type structure via the dressed states formed by the qubit-resonator system [30,31] or making a metastable state protected by quantum interference effects [32] to achieve EIT. Although an artificial Λ-type atom can be made, the EIT-based microwave memory is still challenging to realize. In the experiments of Refs. [30,32], EIT was observed with the probe light driving the one-photon transition from the metastable state to the excited state. The coupling light drives a two-photon process from the ground state to the excited state (dipole-forbidden transition). The strong off-resonant two-photon drive induces a significant shift to the qubit transition frequency due to the Stark effect [30,32–34]. The protocol is not easy to apply to microwave memory because the shift is varied while turning off the coupling light. In the experiment

*Corresponding author: yfuchen@ncu.edu.tw

of Ref. [31], the optimization of the strength of the coupling light is about 1 MHz, limited by its design. The transparency bandwidth is not enough to store an order of 100-ns or shorter pulse. One feasible proposal to realize the microwave memory uses a pair of coupled resonant transmon qubits to form a Λ-type atom [35]. Via modulating the transition frequency in one of the qubits, the population in the superradiant state becomes in the subradiant state. However, the flux noise becomes the main decoherence source of the subradiant state (metastable state) and is hard to avoid. Qubit metamaterial, composed of a linear array of superconducting atoms, also shows the possibility of demonstrating EIT microwave memory [36–38].

In this paper we propose an on-chip detuned quantum circuit (DQC) composed of a transmon qubit [39] and a resonator to store and retrieve microwaves by EIT. By parametrically modulating the qubit transition frequency, we activate the first-order dipole-forbidden sideband transition of the transmon qubit [40] and the DQC exhibits a Λ-type structure. In particular, the state transfer within the DQC via the parametric modulation is widely used in two-qubit gates in superconducting circuits [41–44]. However, simultaneously applying the weak direct probe light and the strong parametric modulation on the qubit has not been thoroughly studied. Benefiting from the frequency tunability of the qubit, we could set the qubit at the linear frequency tuning regime to avoid the frequency shift when applying the parametric modulation. Our scheme behaves like traditional Λ-type EIT and the width of the transparency window can be up to 2.7 MHz according to the parameter choice. Furthermore, the metastable state of the DQC, created by the high-quality resonator, is immune to the flux noise. The loss rate of the memory can be reduced to 5.70 kHz by applying the Purcell filter [45]. Here we demonstrate that with parametric modulation, an EIT effect on the probe light can be observed. Adiabatically turning off the parametric modulation, an order of 100-ns probe pulse can be stored with only one qubit.

The paper is organized as follows. In Sec. II we describe the circuit of the DQC and the effect of the parametric modulation. In Sec. III we numerically calculate the response of the probe light with the parametric modulation. The optical response is EIT, which is confirmed by the populations of the DQC and Akaike's information criterion [29,46]. In Sec. IV we discuss the effect of the Purcell filter and numerically observe the slow light and stored light phenomena. A brief summary is presented in Sec. V.

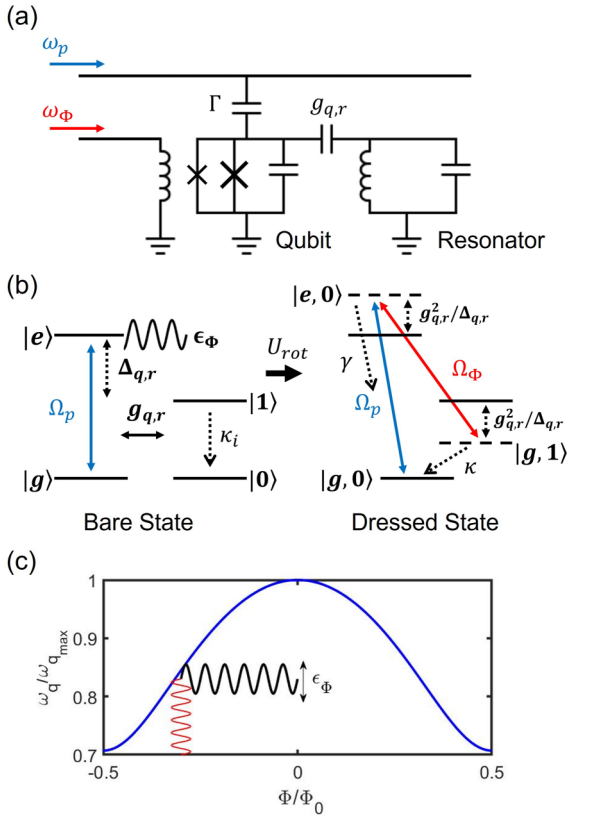

FIG. 1. Schematic diagram of the DQC in waveguide quantum electrodynamics. (a) The qubit is coupled to the one-dimensional open transmission line and a far-detuned resonator. The weak probe light with frequency ω_p is injected onto the transmission line and interacts with the qubit. The parametric modulation with frequency ω_Φ goes through the flux line to modulate the qubit transition frequency ω_q^0. (b) Energy-level diagram of the bare states (left) and the dressed states (right). Dashed lines denote the dressed energy levels and have a Λ-type-like energy-level diagram, where the state $|g, 1\rangle$ is the metastable state. The weak probe light Ω_p (blue arrow) becomes transparent when the parametric modulation Ω_Φ is turned on (red arrow). (c) Qubit transition frequency ω_q versus flux Φ (blue curve). The qubit is biased at the linear slope regime. The red sinusoidal wave indicates the flux modulation which results in the modulation of $\omega_q(t)$ (black wave).

II. MODEL

A. System

Our proposed DQC design is shown in Fig. 1(a). The tunable transmon qubit with transition frequency ω_q^0 is strongly coupled to the one-dimensional open transmission line and to the high-quality resonator with resonant frequency ω_r. The incoming resonant probe light $\omega_p \approx \omega_q^0$ is fully reflected by the qubit as long as the probe Rabi frequency Ω_p is weaker than Γ and the total decoherence rate $\gamma = \gamma_\phi + \Gamma/2$, where Γ and γ_ϕ are the relaxation rate and the pure dephasing rate of the qubit [28,47–49]. The resonator is placed far away from the transmission line, the direct coupling between them can be neglected, and only the internal loss rate κ_i of the resonator is taken into account.

In addition, the DQC is operated in the dispersive regime. The detuning $\Delta_{q,r} = \omega_q^0 - \omega_r$ between the qubit and the resonator is much larger than their coupling strength $g_{q,r}/2\pi = 90$ MHz. In our simulation, we set the system parameters $\omega_q^0/2\pi = 6$ GHz, $\omega_r/2\pi = 4.5$ GHz, $\Gamma/2\pi = 20.736$ MHz, $\gamma_\phi/2\pi = 0.1$ MHz, and $\kappa_i/2\pi = 4.5$ kHz corresponding to the resonator internal quality factor $Q_i = 10^6$. These values are standard for recent superconducting circuit architecture. According to the Purcell effect, the loss rate of the resonator κ is enhanced approximately to $[1 - (g_{q,r}/\Delta_{q,r})^2]\kappa_i + (g_{q,r}/\Delta_{q,r})^2\Gamma$ [50]. The modified $\kappa/2\pi$ is about 79 kHz.

Figure 1(b) shows the three lowest-energy dressed states of the DQC, where $|g, n\rangle$ ($|e, n\rangle$) means the qubit is mainly at the ground (excited) state and the resonator is at the n-photon

Fock state. The state $|g, 1\rangle$ acts as the metastable state for EIT due to the sufficiently small κ compared to γ as long as the forbidden sideband transition from the state $|e, 0\rangle$ to $|g, 1\rangle$ can be turned on [40].

B. Effective Λ-type atom manipulated by parametric modulation

The sideband transition is allowed by parametrically modulating the qubit transition frequency with a frequency $\omega_\Phi \approx \Delta_{q,r}$ [see Fig. 1(c)]. The transition frequency of the tunable transmon qubit with a superconducting quantum interference device (SQUID) is written as $\omega_q(\Phi) = \sqrt{8E_cE_J(\Phi/\Phi_0)} - E_c$, where E_c denotes the charging energy, $E_J(\Phi/\Phi_0)$ denotes the flux-dependent Josephson energy, and Φ_0 is the flux quantum. Modulating the flux Φ results in $E_J(t) = E_J^{\max}\cos[\pi\Phi(t)/\Phi_0]\sqrt{1+d^2\tan^2[\pi\Phi(t)/\Phi_0]}$, where $E_J^{\max}$ is the maximum Josephson energy and d represents the ratio of junction asymmetry. The asymmetry ratio $d = 0.5$ is considered. The asymmetric SQUID design not only reduces the flux noise but also provides a linear slope for the modulation. By biasing and modulating the qubit at the linear slope regime, the qubit transition frequency varying with time is written as

$$\omega_q(t) \approx \omega_q^0 + \frac{\epsilon_\Phi}{2}\sin(\omega_\Phi t), \tag{1}$$

where ϵ_Φ is the resulting parametric modulation magnitude of the transition frequency. The Hamiltonian of the DQC with the parametric modulation and the probe light can be described by the driven Jaynes-Cummings model,

$$\begin{aligned} H(t) =& \omega_q(t)\sigma^\dagger\sigma + \omega_r a^\dagger a + g_{q,r}(a^\dagger\sigma + \sigma^\dagger a) \\ &+ \Omega_p\cos(\omega_p t)(\sigma + \sigma^\dagger), \end{aligned} \tag{2}$$

where σ ($\sigma^\dagger$) is the lowering (raising) operator for the qubit and a ($a^\dagger$) is the lowering (raising) operator for the resonator. To observe the sideband transition, we apply the unitary transform $U_{\rm rot}$ in the rotating frame of instantaneous qubit transition frequency and resonator frequency,

$$U_{\rm rot} = \exp\left[i\left(\omega_q^0 t - \frac{\epsilon_\Phi}{2\omega_\Phi}\cos(\omega_\Phi t)\right)\sigma^\dagger\sigma + i\omega_r a^\dagger a t\right]. \tag{3}$$

We also assume that the probe light is resonant with the qubit and $\epsilon_\Phi \ll 2\omega_\Phi$. The latter condition ensures that the motion averaging takes place and has a negligible effect on Ω_p [35,51]. We define the Hamiltonian after the unitary transformation as H'. Neglecting the fast rotating terms, the Hamiltonian is given as (see Appendix A)

$$\begin{aligned} H'(t) =& \frac{\Omega_p}{2}(\sigma + \sigma^\dagger) + g_{q,r}\sum_{n=-\infty}^{\infty} J_n\left(\frac{\epsilon_\Phi}{2\omega_\Phi}\right) \\ &\times (i^n e^{i(n\omega_\Phi - \Delta_{q,r})t}a^\dagger\sigma + \text{H.c.}), \end{aligned} \tag{4}$$

where J_n is the Bessel function of the first kind. In the dispersive regime, ω_q^0 and ω_r are modified by the Lamb shift and a qubit state-dependent shift to $\tilde{\omega}_q^0 = \omega_q^0 + g_{q,r}^2/\Delta_{q,r}$ and $\tilde{\omega}_r = \omega_r + (g_{q,r}^2/\Delta_{q,r})\sigma_z$, where σ_z is the Pauli Z operator. Operating at the weak probe regime ($\Omega_p \ll \Gamma, \gamma$), the qubit is nearly at the ground state. When $\omega_\Phi = \tilde{\Delta}_{q,r} \equiv \tilde{\omega}_q^0 - \tilde{\omega}_r = \omega_q^0 - \omega_r + 2g_{q,r}^2/\Delta_{q,r}$, the parametric modulation induced Rabi frequency Ω_Φ is mainly governed by [41]

$$\Omega_\Phi = 2g_{q,r}J_1\left(\frac{\epsilon_\Phi}{2\omega_\Phi}\right). \tag{5}$$

The resulting Hamiltonian in Eq. (4) with the near-resonant parametric modulation is indeed identical to a Λ-type atom interacting with the probe and the coupling light. In the next section, the steady-state numerical results will show that EIT can be observed in the DQC.

III. PARAMETRIC-MODULATION-INDUCED TRANSPARENCY

To observe the optical response of the probe light passing through the DQC with the parametric modulation, we numerically calculate the expectation value $\langle\sigma\rangle$ from Eq. (2). We simplify the calculation by choosing the rotating frame at ω_p and neglecting the fast rotating terms. The Hamiltonian is written as

$$\begin{aligned} H' =& [\omega_q(t) - \omega_p]\sigma^\dagger\sigma + (\omega_r - \omega_p)a^\dagger a \\ &+ g_{q,r}(a^\dagger\sigma + \sigma^\dagger a) + \frac{\Omega_p}{2}(\sigma^\dagger + \sigma). \end{aligned} \tag{6}$$

The dynamics of the DQC is governed by the Lindblad master equation

$$\dot{\rho} = -i[H', \rho] + \frac{\Gamma}{2}\mathcal{D}[\sigma]\rho + \frac{\kappa_i}{2}\mathcal{D}[a]\rho + \gamma_\phi\mathcal{D}[\sigma^\dagger\sigma]\rho, \tag{7}$$

where $\mathcal{D}[\mathcal{O}]\rho = 2\mathcal{O}\rho\mathcal{O}^\dagger - \rho\mathcal{O}^\dagger\mathcal{O} - \mathcal{O}^\dagger\mathcal{O}\rho$. Here $\rho(t)$ is the density matrix and it is calculated by QUTIP [52]. The steady-state optical response is characterized by the transmission coefficient t_c of the scattered probe light [47,53]

$$t_c = 1 + i\frac{\Gamma}{\Omega_p}\langle\sigma\rangle. \tag{8}$$

In our simulation, $\Omega_p = 0.01\Gamma$ and $\omega_\Phi = \tilde{\Delta}_{q,r}$ are fixed. $\mathrm{Re}(t_c)$ is plotted as a function of ω_p and ϵ_Φ in Fig. 2(a). Line cuts of Fig. 2(a) are depicted in Fig. 2(b). Without the parametric modulation, an absorption response is obtained and the minimum of $\mathrm{Re}(t_c)$ is at $\omega_p = \tilde{\omega}_q^0 = 6.0054$ GHz due to the Lamb shift effect. With the parametric modulation, the splitting structure appears. To compare the splitting magnitude with Eq. (5), we fit the data to the analytical transmission coefficient of a Λ-type atom with the probe and resonant coupling lights. The analytical form is written as [54,55]

$$t_c^a = 1 + i\frac{\frac{\Gamma}{2}\left(\tilde{\omega}_q^0 - \omega_p - i\frac{\kappa}{2}\right)}{\left(\tilde{\omega}_q^0 - \omega_p - i\frac{\kappa}{2}\right)\left(\tilde{\omega}_q^0 - \omega_p - i\gamma\right) - \left(\frac{\Omega_\Phi^2}{4}\right)}, \tag{9}$$

which describes both ATS and EIT phenomena in the driven Λ-type atom. The fitting results for Ω_Φ are shown in Fig. 2(c) and are consistent with Eq. (5).

With the condition $\Omega_\Phi < \gamma - \kappa/2$ [29,56], the interference effect occurs and the DQC would not be populated to the excited state $|e, 0\rangle$ but stays in the dark state polariton as [57,58]

$$|d\rangle = e^{-|\alpha|^2}\sum\frac{\alpha^n}{\sqrt{n!}}|g, n\rangle = |g\rangle|\alpha\rangle, \tag{10}$$

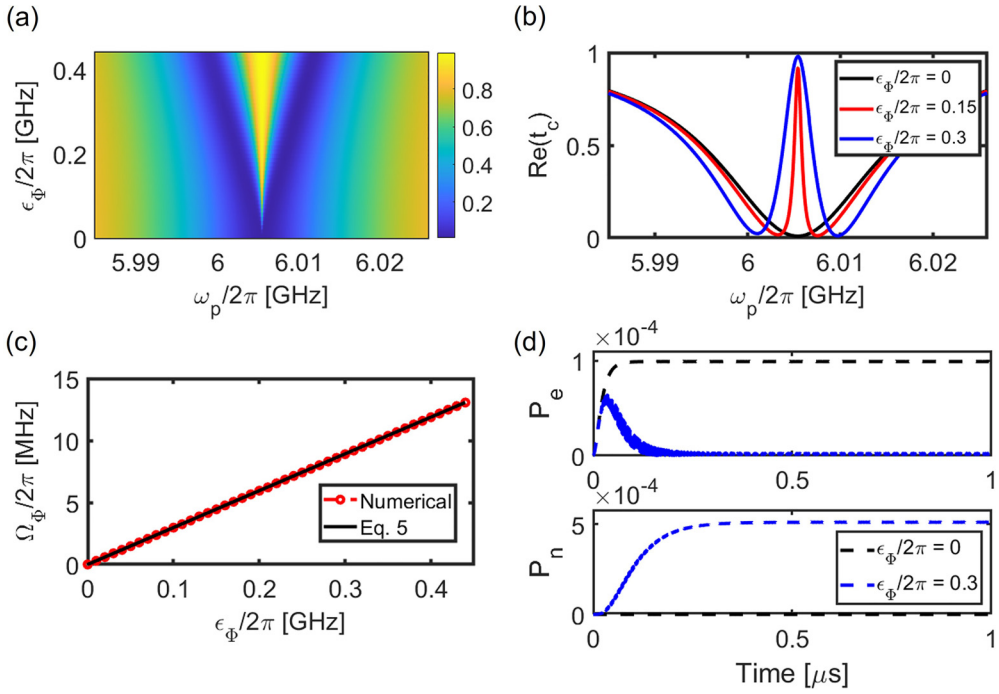

FIG. 2. Steady-state response of the DQC with the probe light and parametric modulation. (a) Real part of the transmission coefficient Re(t_c) varies with the probe light frequency ω_p and the modulation magnitude ϵ_Φ. The color in (a) denotes the magnitude of Re(t_c). Line cuts are shown in (b). The splitting magnitude is proportional to ϵ_Φ. (c) Plot of Ω_Φ as a function of ϵ_Φ. Red open circles are the fitting Rabi frequency Ω_Φ of the data in (a). The black solid line is calculated from Eq. (5). (d) Population P_e of the qubit (top plot) and P_n of the resonator (bottom plot) with the resonant probe light and parametric modulation. The black (blue) dashed line indicates the situation without (with) the parametric modulation.

where $|\alpha| = |-i\Omega_p/\Omega_\Phi|$ is the magnitude of the coherent state in the resonator. The derivation is given in Appendix B. In particular, with $\Omega_p \ll \Omega_\Phi$, $|d\rangle \approx |g, 0\rangle$. To confirm that the interference effect occurs in the DQC, the time evolutions of its populations with and without the parametric modulation are depicted in Fig. 2(d). The parameters we use are $\Omega_p = 0.01\Gamma$ and $\Omega_\Phi/2\pi \approx 8.9$ MHz. In the absence of the parametric modulation, the population of the excited state of the qubit P_e is populated and the population of the photon numbers of the resonator P_n is weak enough to be neglected due to the large detuning with the qubit. With the parametric modulation applied, P_e decreases to 0 rapidly and P_n is comparable to $|\alpha|^2 \approx 5 \times 10^{-4}$ because the DQC is in the dark state polariton.

In the real experiment, we can fit the splitting steady-state Re(t_c) with different fitting models and apply Akaike's information criterion (AIC) [29,46] to objectively determine which model fits better. The transmission profile fitting model for EIT has a structure of a broad Lorentzian absorption dip with a narrow Lorentzian peak

$$t_c^{\mathrm{EIT}} = 1 - \left(\frac{C_+^2}{(\gamma_+^2 + \tilde{\Delta}^2)} - \frac{C_-^2}{(\gamma_-^2 + \tilde{\Delta}^2)} \right) \tag{11}$$

and ATS has two Lorentzians with equal width but different peak centers

$$t_c^{\mathrm{ATS}} = 1 - \left(\frac{C^2}{\gamma^2 + (\tilde{\Delta} - \delta)^2} + \frac{C^2}{\gamma^2 + (\tilde{\Delta} + \delta)^2} \right). \tag{12}$$

The fitting results for $\epsilon_\Phi/2\pi = 0.3$ GHz are shown in Fig. 3(a), and the EIT model is more consistent with the

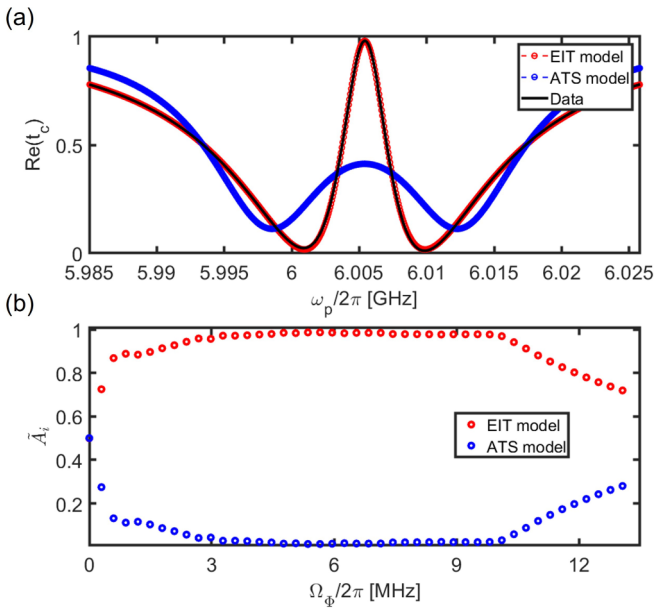

FIG. 3. Different fitting models and AIC. (a) Plot of Re(t_c) vs $\omega_p/2\pi$ with $\Omega_\Phi/2\pi \approx 8.9$ GHz. The black solid line is the numerical data. Red (blue) dashed lines with open circles denote the fitting result with the EIT (ATS) model. (b) Plot of weight $\tilde{A}_i$ vs different Ω_Φ. Red (blue) open circles indicate $\tilde{A}_i$ obtained with the EIT (ATS) model.

numerical data due to the condition $\Omega_\Phi < \gamma - \kappa/2$. The per point weight $\tilde{A}_i$ of AIC is defined as

$$\tilde{A}_{\rm EIT} = \frac{e^{-I_{\rm EIT}/2}}{e^{-I_{\rm EIT}/2} + e^{-I_{\rm ATS}/2}}, \tag{13a}$$

$$\tilde{A}_{\rm ATS} = 1 - \tilde{A}_{\rm EIT}, \tag{13b}$$

where $I_i = [N \log(R/N) + 2k_i]/N$, with i denoting the model used, R the fitting residual, N the number of fitting points, and k_i the number of the fitting parameters. The results of AIC for different Ω_Φ are plotted in Fig. 3(b). Due to the fixed frequency resolution in the data, the EIT window is too small to distinguish with weak Ω_Φ. In the regime $\Omega_\Phi < \gamma - \kappa/2$, the EIT model is more consistent with the data. For stronger Ω_Φ, the ATS model starts to depict the optical response.

We show that under the appropriate parametric modulation, the transparency effect can be realized. To further make the system suitable for storing information, the inverse Purcell effect should be suppressed. In the next section we include a Purcell filter to engineer the spectral density of the environment to enhance the memory lifetime.

IV. STORING AND RETRIEVING MICROWAVES WITH PURCELL FILTER

A. Description of the Purcell filter

We add a broadband $\lambda/2$ resonator with equal loss rates for the input and output as a Purcell filter [45] [see Fig. 4(a)]. The Purcell filter frequency $\omega_F/2\pi = 6.0054$ GHz is designed to be resonant with the dressed qubit transition frequency $\tilde{\omega}_q^0$, and the total loss rate $\kappa_F/2\pi = 250$ MHz is much larger than the coupling between the filter and the qubit $g_{F,q}/2\pi = 36$ MHz. With the filter, the spectral density of the environment is frequency dependent. Reference [45] gives the effective loss rate $\kappa_{\rm eff}$ with different frequencies ω_i:

$$\kappa_{\rm eff} = \frac{4{g_{F,q}}^2}{\kappa_F} \frac{1}{1 + [2(\omega_i - \omega_F)/\kappa_F]^2}. \tag{14}$$

The effective loss rate near $\tilde{\omega}_q^0$ is about $\kappa_q/2\pi = 20.736$ MHz and at the resonator frequency ω_r is about $\kappa_r/2\pi = 141$ kHz. The modified loss rate $\kappa \approx [1 - (g_{q,r}/\Delta_{q,r})^2]\kappa_i + (g_{q,r}/\Delta_{q,r})^2\kappa_r \approx 2\pi \times 4.99$ kHz is suppressed about a factor of 15 compared to the case without the filter. In this case, the memory lifetime is nearly dominated by the quality of the resonator.

We numerically calculate the optical response of the DQC with the filter. The probe light ω_p is now directly applied on the filter and induces a new probe Rabi frequency Ω_p^F. With the condition $g_{F,q} < \kappa_F/2$, the applied probe light $\omega_p = \omega_F$ to the Purcell filter can directly drive the qubit because $g_{F,q}$ is not large enough to resolve the vacuum Rabi splitting with eigenstates $(|0^F, e\rangle + |1^F, g\rangle)/\sqrt{2}$ and $(|0^F, e\rangle - |1^F, g\rangle)/\sqrt{2}$, where n^F denotes the Fock state in the filter. Therefore, an electromagnetically induced absorption occurs due to the destructive interference effect, and the qubit is directly interacting with the probe light [59,60]. Note that $\Omega_p^F \neq \Omega_p$ and their relation is [45]

$$\Omega_p = -i\Omega_p^F g_{F,q}/(\kappa_F/2 + i\Delta_{F,p}), \tag{15}$$

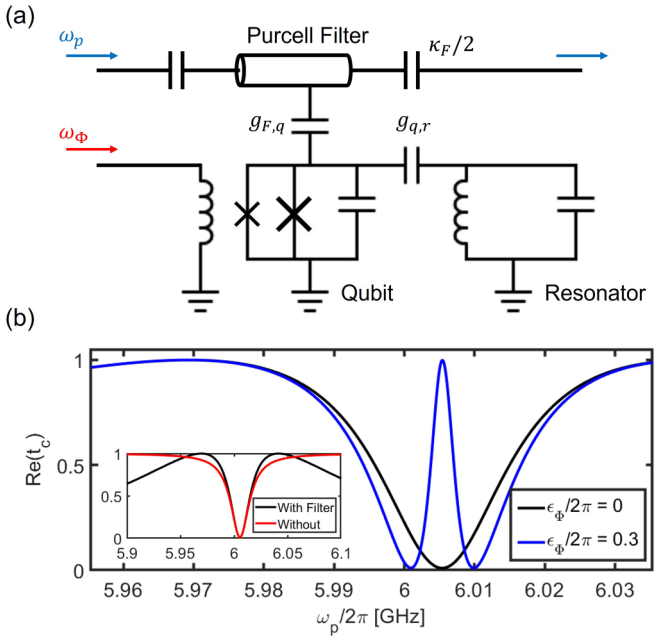

FIG. 4. Purcell filter with the DQC. (a) Circuit diagram. The qubit is resonant with the filter and is directly coupled to the filter. The other parameters of the DQC are the same as in Fig. 1(a). The probe light ω_p is now directly driving the filter. (b) Real part of the transmission coefficient Re(t_c) as a function of ω_p. The blue solid line denotes the transparency effect caused by the parametric modulation. The black solid line denotes the transmission profile without the parametric modulation. The inset shows Re(t_c) without the parametric modulation with a wider frequency range. The black (red) solid line denotes the transmission profile with (without) the filter.

where $\Delta_{F,p} = \omega_F - \omega_p$. In the calculation, we set $\Omega_p^F \approx 0.035\Gamma$ with $\Delta_{F,p} = 0$. This magnitude of Ω_p^F results in the same magnitude $\Omega_p \approx 0.01\Gamma$ on the qubit. The Hamiltonian in the rotating frame at ω_p (neglect the fast rotating terms) now is

$$H_F' = (\omega_F - \omega_p)b^\dagger b + [\omega_q(t) - \omega_p]\sigma^\dagger\sigma + (\omega_r - \omega_p)a^\dagger a + g_{F,q}(b^\dagger\sigma + \sigma^\dagger b) + g_{q,r}(a^\dagger\sigma + \sigma^\dagger a) + \frac{\Omega_p^F}{2}(b^\dagger + b), \tag{16}$$

where b ($b^\dagger$) is the lowering (raising) operator for the filter. We consider κ_F in the master equation

$$\dot{\rho} = -i[H_F', \rho] + \frac{\kappa_F}{2}\mathcal{D}[b]\rho + \frac{\kappa_i}{2}\mathcal{D}[a]\rho + \gamma_\phi\mathcal{D}[\sigma^\dagger\sigma]\rho. \tag{17}$$

The optical response is associated with the expectation value $\langle b\rangle$. Applying the input-output theory [61,62], the transmission coefficient t_c of the scattered probe light out from the filter is given as

$$t_c = \sqrt{\frac{\kappa_F}{2}}\langle b\rangle/\alpha_{\rm in}, \tag{18}$$

where $\alpha_{\rm in} = i\Omega_p^F/2\sqrt{\kappa_F/2}$ is the input coherent field. The steady-state results Re(t_c) are shown in Fig. 4(b). The inset

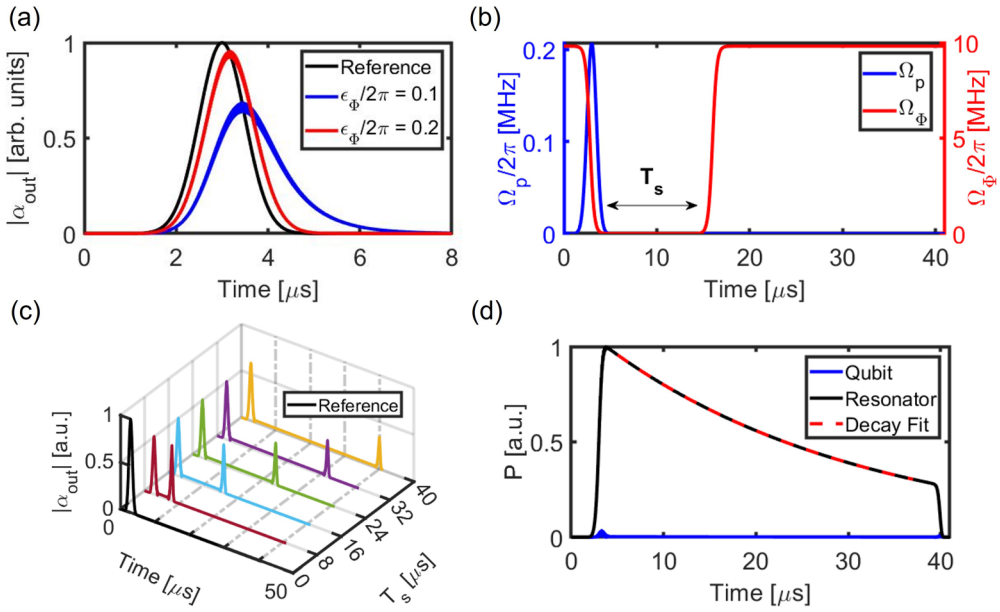

FIG. 5. Pulsed light storage. (a) Slow light experiment. Here $|\alpha_{\text{out}}|$ is the absolute value of the magnitude of the output coherent pulse. The x axis is the evolution time. A 500-ns Gaussian probe pulse arrives after a constant parametric modulation. The $|\alpha_{\text{in}}|$ is defined as the reference pulse (black curve). The pulse with nonzero ϵ_Φ is slower than the reference pulse. (b) EIT-based microwave memory protocol. The red (blue) solid line denotes Ω_Φ (Ω_p). Here T_s is the storing time. A 500-ns Gaussian probe pulse arrives before the parametric modulation is adiabatically turned off. The pulse is partially stored in the resonator. After the parametric modulation is turned on, the pulse is retrieved by the filter. (c) EIT-based microwave memory result. Different colors denote the different T_s in (b). The first Gaussian pulse indicates the noncaptured pulse and the second one is the retrieved pulse. (d) Population of the qubit and resonator versus time evolution.

in Fig. 4(b) shows the transmission profile with the filter that has a broadband Lorentzian structure. A dip occurs when $\omega_p \approx \omega_F$ due to the absorption of the qubit. With the resonant parametric modulation ($\omega_\Phi = \tilde{\Delta}_{q,r}$), the transparency of the probe light occurs at $\omega_p = \tilde{\omega}_q^0$.

B. Demonstration of storing microwaves

In this section we numerically calculate the response of the probe pulse after passing through the circuit in Fig. 4(a) with the parametric modulation. The carrier frequency of the pulse is set at $\omega_p = \tilde{\omega}_q^0$. The magnitude of the output coherent pulse response $|\alpha_{\text{out}}| = |\sqrt{\frac{\kappa_F}{2}}\langle b\rangle|$ is measured [63].

Before demonstrating the stored light phenomenon via the parametric modulation induced transparency, we first observe the slow light effect of the probe pulse with the continuing constant parametric modulation. A Gaussian probe pulse with duration $\tau_d = 500$ ns and amplitude $\Omega_p^F \approx 0.035\Gamma$, expressed as $\Omega_p^F \exp(-t^2/2{\tau_d}^2)$, is sent into the system and is slowed down due to the great change of the dispersion (not shown). The modified dispersion is a function of the magnitude ϵ_Φ, where the dispersion changes more sharply with weaker ϵ_Φ. As shown by the numerical results in Fig. 5(a), the probe pulse becomes much slower with weaker ϵ_Φ. Note that the spectral bandwidth of the probe pulse should be smaller than the full width at half maximum (FWHM) of the transparency window γ_{EIT} to prevent the nonresonant absorption of the probe pulse. With the negligible κ, γ_{EIT} can be described as [11]

$$\gamma_{\text{EIT}} \approx \frac{\sqrt{\ln 2}}{2}\frac{\Omega_\Phi^2}{\sqrt{\Gamma\gamma}}, \tag{19}$$

which is limited by the decoherence rates of the transmon qubit and the magnitude of Ω_Φ. In the stored light simulation, $\Omega_\Phi/2\pi \approx 9.8$ MHz (corresponding to $\epsilon_\Phi/2\pi = 0.33$ GHz) is set to have $\gamma_{\text{EIT}}/2\pi \approx 2.7$ MHz, but still in the EIT regime, which is larger than the spectral FWHM of the probe pulse approximately equal to 0.75 MHz. Here we have assumed that the optical depth D of the single atom is 2 [49] and D is verified by fitting the probe pulse delay time T_d [3],

$$T_d = \frac{D\kappa_q}{\Omega_\Phi^2}. \tag{20}$$

The stored light phenomenon is achieved by adiabatically turning off the parametric modulation before the probe pulse leaves the medium [see Fig. 5(b)]. In this process, the DQC would stay in the dark state polariton and adiabatically transfers from $|d\rangle \approx |g, 0\rangle$ to $|d\rangle \approx |g, 1\rangle$ (Here we neglect the basis of the filter.) After storing the probe pulse for a time period T_s, the parametric modulation is then turned on to retrieve it. The results are shown in Fig. 5(c). After turning off the parametric modulation, part of the probe pulse is stored in the resonator and the other part is not captured. With a longer storing time T_s, the amplitude of the retrieved pulse becomes weaker due to the coherent properties of the resonator. The population of the qubit and resonator with the stored light protocol is shown in Fig. 5(d). The population P_e of the qubit is only being populated slightly at the beginning of the experiment, which might be due to the nonzero absorption of the nonresonant components of the probe pulse. The probe pulse is then stored in the resonator. We fit the decay of the population P_n of the resonator at about $\kappa/2\pi \approx 5.70$ kHz. The

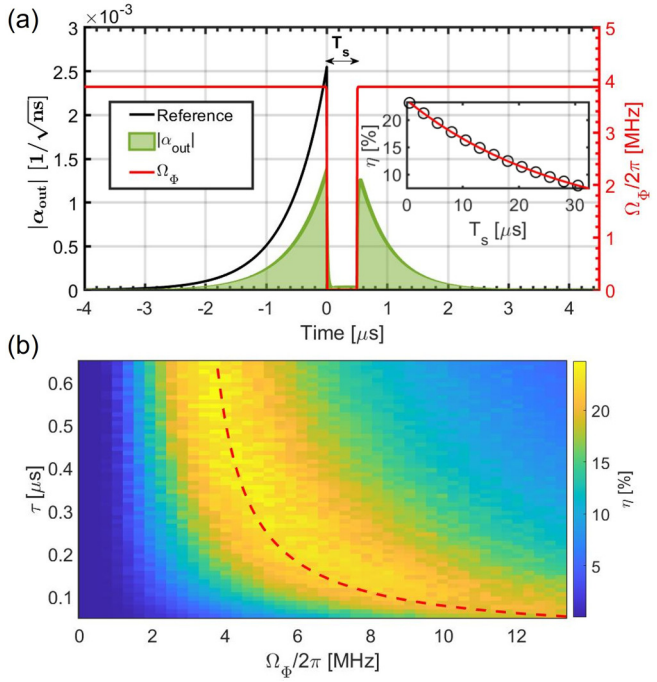

FIG. 6. Storage efficiency η of the exponential rising probe pulse. (a) Time evolution of the storage process. The parameters are $\tau = 0.58$ μs and $\Omega_\Phi/2\pi \approx 3.6$ MHz. Here $|\alpha_{\rm out}|$ is the absolute value of the magnitude of the output coherent pulse. The black solid line denotes the input probe pulse $|\alpha_{\rm in}|$, defined as the reference pulse. The green solid line denotes the output probe pulse with the switching off and on of the parametric modulation (red solid line). Part of the probe pulse is not captured when switching off the parametric modulation at $t = 0$. The other part is stored and retrieved at 0.5 μs. The inset shows η as a function of T_s. The decay rate is close to 5.70 kHz. (b) Plot of η as a function of τ and Ω_Φ. The color indicates the magnitude of η. The red dashed line indicates the condition for the optimal η.

result of the memory lifetime is close to the expected value from the circuit parameters.

We also systemically study the storage efficiency η. In contrast to an input Gaussian pulse, an exponential rising probe pulse, that can be separated from its slow light, is used. Therefore, we specifically investigate storage and retrieval with an explicit identification of storage time as indicated by the black arrow in Fig. 6(a). The input pulse ends at $t = 0$ and is expressed as

$$\Omega_p^F(t) = \Omega_p^F e^{t/\tau}\Theta(-t), \tag{21}$$

where τ is the characteristic rising time scale and Θ is the Heaviside step function. The parametric modulation is adiabatically turned off at $t = 0$ and on at $T_s = 0.5$ μs [see Fig. 6(a)]. The storage efficiency η, as a function of τ and Ω_Φ, is calculated as

$$\eta = \frac{\int_{T_s}^{\infty} |\alpha_{\rm out}|^2 dt}{\int_{-\infty}^{0} |\alpha_{\rm in}|^2 dt}. \tag{22}$$

The result is shown in Fig. 6(b). As τ is small, Ω_Φ should be large to cover the frequency bandwidth of the short probe pulse to reach high η. When τ becomes larger, the best η happens at weaker Ω_Φ. The result shows that the optimal η of the certain τ happens at the specific ratio of the pulse frequency bandwidth to the EIT window. We fit $\Omega_\Phi/2\pi$ for the optimal η as a linear function of $1/\tau$ and observe that the optimal η occurs on the condition of $\Omega_\Phi/2\pi = 0.55\tau^{-1} + 2.92$ in our system [see Fig. 6(b)]. Note that η can be improved by making a more proper control parameter and the shape of the probe pulse [64,65].

V. CONCLUSION

We have proposed a realization of EIT using a qubit-resonator system along with the parametric modulation. The optical response of the probe light passing through the qubit with the parametric modulation was obtained numerically, and therein we observed and confirmed the phenomenon of EIT. To increase the coherent time of the metastable state, we added the Purcell filter to design the environment spectrum. Compared to other EIT schemes in superconducting circuits [30–32], our protocol has a large EIT window, a sufficiently small metastable state loss rate (5.70 kHz), and is suitable for studying EIT-based microwave memory. We numerically showed that our system has the potential to realize an EIT-based microwave memory protocol. The setup is simple and could be used to observe more quantum optics phenomena caused by EIT and even to demonstrate different Λ-type microwave memory protocols [66,67].

ACKNOWLEDGMENTS

The authors are grateful to Yen-Hsiang Lin, Kuan-Hsun Chiang, and Chi-Lun Lee for their helpful discussions. The work was supported by the Ministry of Science and Technology in Taiwan through Grants No. NSTC-110-2112-M-008-024, No. NSTC-111-2112-M-008-022, No. NSTC-110-2112-M-008-027-MY3, No. NSTC-111-2923-M-008-004-MY3, and No. NSTC-111-2639-M-007-001-ASP.

APPENDIX A: EFFECT OF PARAMETRIC MODULATION

The Hamiltonian under unitary transformation is given by $H' = U_{\rm rot} H U_{\rm rot}^\dagger + i\dot{U}_{\rm rot} U_{\rm rot}^\dagger$, with the Hamiltonian H of Eq. (2) and the unitary transform $U_{\rm rot}$ of Eq. (3). Here $U_{\rm rot}$ is chosen such that $i\dot{U}_{\rm rot}U_{\rm rot}^\dagger$ would be canceled out. The remaining terms are

$$H' = g_{q,r} U_{\rm rot}(a^\dagger\sigma + \sigma^\dagger a)U_{\rm rot}^\dagger + \Omega_p \cos(\omega_p t) \times U_{\rm rot}(\sigma + \sigma^\dagger)U_{\rm rot}^\dagger. \tag{A1}$$

By utilizing the Jacobi-Anger expansion $e^{iz\cos(\theta)} = \sum_{n=-\infty}^{\infty} i^n J_n(z) e^{in\theta}$, the first term on the right-hand side of Eq. (A1) is

$$H_1'(t) = g_{q,r} \sum_{n=-\infty}^{\infty} J_n\left(\frac{\epsilon_\Phi}{2\omega_\Phi}\right)(i^n e^{i(n\omega_\Phi - \Delta_{q,r})t} a^\dagger\sigma + \text{H.c.}). \tag{A2}$$

Considering $\omega_p = \omega_q^0$, the second term on the right-hand side of Eq. (A1) is

$$H_2'(t) = \frac{\Omega_p}{2} \sum_{k=-\infty}^{\infty} J_k\left(\frac{\epsilon_\Phi}{2\omega_\Phi}\right)(i^k e^{ik\omega_\Phi t}\sigma + \text{H.c.}). \tag{A3}$$

The parametric modulation is operated at $\epsilon_\Phi \ll 2\omega_\Phi$, so only J_0 survives. With the operating condition, $J_0 \approx 1$ and Ω_p is not affected by the parametric modulation.

APPENDIX B: DERIVATION OF THE DARK STATE POLARITON

Considering the DQC with the resonant probe light and the resonant parametric modulation, the Hamiltonian is given as

$$H' = \frac{\Omega_p}{2}(\sigma + \sigma^\dagger) + \frac{i\Omega_\Phi}{2}(a^\dagger\sigma - a\sigma^\dagger). \tag{B1}$$

In particular, H' is identical to the Hamiltonian of the single-tone driven resonant Jaynes-Cummings system [68], except the coupling between the qubit and the resonator is replaced by Ω_Φ.

We follow the calculation in Ref. [68] to solve the eigenvalue problem. The dark state polariton is associated with the zero-energy state. The eigenstate is the tensor product of the qubit and the resonator states, defined as

$$|\psi\rangle = |g\rangle|\psi^g\rangle + |e\rangle|\psi^e\rangle, \tag{B2}$$

where $|\psi^g\rangle$ and $|\psi^e\rangle$ are the normalized states of the resonator field such that $\langle\psi|\psi\rangle = 1$. We solve the eigenvalue problem with Eqs. (B1) and (B2). By taking the inner products of $\langle e|H'|\psi\rangle$ and $\langle g|H'|\psi\rangle$, we get two equations

$$\begin{aligned} E|\psi^e\rangle + \left(\frac{i\Omega_\Phi}{2}a - \frac{\Omega_p}{2}\right)|\psi^g\rangle = 0, \\ E|\psi^g\rangle - \left(\frac{i\Omega_\Phi}{2}a^\dagger + \frac{\Omega_p}{2}\right)|\psi^e\rangle = 0, \end{aligned} \tag{B3}$$

where E is the eigenenergy, associated with $H'|\psi\rangle = E|\psi\rangle$. We rewrite the second equation by replacing $|\psi^e\rangle$ evaluated from the first equation and obtain

$$\left(a^\dagger - \frac{i\Omega_p}{\Omega_\Phi}\right)\left(a + \frac{i\Omega_p}{\Omega_\Phi}\right)|\psi^g\rangle = \frac{-2iE^2}{\Omega_\Phi}|\psi^g\rangle. \tag{B4}$$

We apply the displacement operator $D(-\frac{i\Omega_p}{\Omega_\Phi})$ to remove the displacement, and Eq. (B4) becomes

$$a^\dagger a|\tilde{\psi}^g\rangle = \frac{-2iE^2}{\Omega_\Phi}|\tilde{\psi}^g\rangle, \tag{B5}$$

where

$$|\tilde{\psi}^g\rangle = D^\dagger\left(-\frac{i\Omega_p}{\Omega_\Phi}\right)|\psi^g\rangle. \tag{B6}$$

The value of $\frac{-2iE^2}{\Omega_\Phi}$ corresponds to the requirement of the discrete number $n = 0, 1, 2, \ldots$, according to Eq. (B5). With $n = 0$, $E = 0$ is the energy of the dark state polariton. We also obtain $|\psi^e\rangle = 0$ from Eq. (B3) with $E = 0$. By inverting Eq. (B6), we get the dark state polariton $|\psi\rangle = |d\rangle$ of Eq. (10).

[1] L.-M. Duan, M. D. Lukin, J. I. Cirac, and P. Zoller, Long-distance quantum communication with atomic ensembles and linear optics, Nature (London) **414**, 413 (2001).

[2] H. J. Kimble, The quantum internet, Nature (London) **453**, 1023 (2008).

[3] M. Fleischhauer, A. Imamoglu, and J. P. Marangos, Electromagnetically induced transparency: Optics in coherent media, Rev. Mod. Phys. **77**, 633 (2005).

[4] G. Hétet, J. J. Longdell, M. J. Sellars, P. K. Lam, and B. C. Buchler, Multimodal Properties and Dynamics of Gradient Echo Quantum Memory, Phys. Rev. Lett. **101**, 203601 (2008).

[5] M. Afzelius, C. Simon, H. de Riedmatten, and N. Gisin, Multimode quantum memory based on atomic frequency combs, Phys. Rev. A **79**, 052329 (2009).

[6] C. Liu, Z. Dutton, C. H. Behroozi, and L. V. Hau, Observation of coherent optical information storage in an atomic medium using halted light pulses, Nature (London) **409**, 490 (2001).

[7] D. F. Phillips, A. Fleischhauer, A. Mair, R. L. Walsworth, and M. D. Lukin, Storage of Light in Atomic Vapor, Phys. Rev. Lett. **86**, 783 (2001).

[8] O. Kocharovskaya, Y. Rostovtsev, and M. O. Scully, Stopping Light via Hot Atoms, Phys. Rev. Lett. **86**, 628 (2001).

[9] W.-T. Liao, C. H. Keitel, and A. Pálffy, All-Electromagnetic Control of Broadband Quantum Excitations Using Gradient Photon Echoes, Phys. Rev. Lett. **113**, 123602 (2014).

[10] S.-W. Su, S.-C. Gou, L. Y. Chew, Y.-Y. Chang, I. A. Yu, A. Kalachev, and W.-T. Liao, Setting a disordered password on a photonic memory, Phys. Rev. A **95**, 061805(R) (2017).

[11] Y.-F. Hsiao, P.-J. Tsai, H.-S. Chen, S.-X. Lin, C.-C. Hung, C.-H. Lee, Y.-H. Chen, Y.-F. Chen, I. A. Yu, and Y.-C. Chen, Highly Efficient Coherent Optical Memory Based on Electromagnetically Induced Transparency, Phys. Rev. Lett. **120**, 183602 (2018).

[12] M. D. Lukin, *Colloquium*: Trapping and manipulating photon states in atomic ensembles, Rev. Mod. Phys. **75**, 457 (2003).

[13] M. Fleischhauer and M. D. Lukin, Dark-State Polaritons in Electromagnetically Induced Transparency, Phys. Rev. Lett. **84**, 5094 (2000).

[14] F. Arute, K. Arya, R. Babbush, D. Bacon, J. C. Bardin, R. Barends, R. Biswas, S. Boixo, F. G. S. L. Brandao, D. A. Buell *et al.*, Quantum supremacy using a programmable superconducting processor, Nature (London) **574**, 505 (2019).

[15] Y. Wu, W.-S. Bao, S. Cao, F. Chen, M.-C. Chen, X. Chen, T.-H. Chung, H. Deng, Y. Du, D. Fan *et al.*, Strong Quantum Computational Advantage Using a Superconducting Quantum Processor, Phys. Rev. Lett. **127**, 180501 (2021).

[16] A. Megrant, C. Neill, R. Barends, B. Chiaro, Y. Chen, L. Feigl, J. Kelly, E. Lucero, M. Mariantoni, P. J. J. O'Malley *et al.*, Planar superconducting resonators with internal quality factors above one million, Appl. Phys. Lett. **100**, 113510 (2012).

[17] M. Reagor, H. Paik, G. Catelani, L. Sun, C. Axline, E. Holland, I. M. Pop, N. A. Masluk, T. Brecht, L. Frunzio *et al.*, Reaching 10 ms single photon lifetimes for superconducting aluminum cavities, Appl. Phy. Lett. **102**, 192604 (2013)

[18] M. Reagor, W. Pfaff, C. Axline, R. W. Heeres, N. Ofek, K. Sliwa, E. Holland, C. Wang, J. Blumoff, K. Chou *et al.*,

Quantum memory with millisecond coherence in circuit QED, Phys. Rev. B **94**, 014506 (2016).

[19] R. K. Naik, N. Leung, S. Chakram, P. Groszkowski, Y. Lu, N. Earnest, D. C. McKay, J. Koch, and D. I. Schuster, Random access quantum information processors using multimode circuit quantum electrodynamics, Nat. Commun. **8**, 1904 (2017).

[20] S. Chakram, A. E. Oriani, R. K. Naik, A. V. Dixit, K. He, A. Agrawal, H. Kwon, and D. I. Schuster, Seamless High-Q Microwave Cavities for Multimode Circuit Quantum Electrodynamics, Phys. Rev. Lett. **127**, 107701 (2021).

[21] A. Krasnok, P. Dhakal, A. Fedorov, P. Frigola, M. Kelly, and S. Kutsaev, Advancements in superconducting microwave cavities and qubits for quantum information systems, arXiv:2304.09345.

[22] Y. Yin, Y. Chen, D. Sank, P. J. J. O'Malley, T. C. White, R. Barends, J. Kelly, E. Lucero, M. Mariantoni, A. Megrant *et al.*, Catch and Release of Microwave Photon States, Phys. Rev. Lett. **110**, 107001 (2013).

[23] J. Wenner, Y. Yin, Y. Chen, R. Barends, B. Chiaro, E. Jeffrey, J. Kelly, A. Megrant, J. Y. Mutus, C. Neill *et al.*, Catching Time-Reversed Microwave Coherent State Photons with 99.4% Absorption Efficiency, Phys. Rev. Lett. **112**, 210501 (2014).

[24] E. Flurin, N. Roch, J. D. Pillet, F. Mallet, and B. Huard, Superconducting Quantum Node for Entanglement and Storage of Microwave Radiation, Phys. Rev. Lett. **114**, 090503 (2015).

[25] Z. Bao, Z. Wang, Y. Wu, Y. Li, C. Ma, Y. Song, H. Zhang, and L. Duan, On-Demand Storage and Retrieval of Microwave Photons Using a Superconducting Multiresonator Quantum Memory, Phys. Rev. Lett. **127**, 010503 (2021).

[26] A. R. Matanin, K. I. Gerasimov, E. S. Moiseev, N. S. Smirnov, A. I. Ivanov, E. I. Malevannaya, V. I. Polozov, E. V. Zikiy, A. A. Samoilov, I. A. Rodionov, and S. A. Moiseev, Toward Highly Efficient Multimode Superconducting Quantum Memory, Phys. Rev. Appl. **19**, 034011 (2023).

[27] A. A. Abdumalikov, Jr., O. Astafiev, A. M. Zagoskin, Y. A. Pashkin, Y. Nakamura, and J. S. Tsai, Electromagnetically Induced Transparency on a Single Artificial Atom, Phys. Rev. Lett. **104**, 193601 (2010).

[28] I.-C. Hoi, C. M. Wilson, G. Johansson, T. Palomaki, B. Peropadre, and P. Delsing, Demonstration of a Single-Photon Router in the Microwave Regime, Phys. Rev. Lett. **107**, 073601 (2011).

[29] P. M. Anisimov, J. P. Dowling, and B. C. Sanders, Objectively Discerning Autler-Townes Splitting from Electromagnetically Induced Transparency, Phys. Rev. Lett. **107**, 163604 (2011).

[30] S. Novikov, T. Sweeney, J. E. Robinson, S. P. Premaratne, B. Suri, F. C. Wellstood, and B. S. Palmer, Raman coherence in a circuit quantum electrodynamics lambda system, Nat. Phys. **12**, 75 (2016).

[31] J. Long, H. S. Ku, X. Wu, X. Gu, R. E. Lake, M. Bal, Y.-X. Liu, and D. P. Pappas, Electromagnetically Induced Transparency in Circuit Quantum Electrodynamics with Nested Polariton States, Phys. Rev. Lett. **120**, 083602 (2018).

[32] A. M. Vadiraj, A. Ask, T. G. McConkey, I. Nsanzineza, C. W. S. Chang, A. F. Kockum, and C. M. Wilson, Engineering the level structure of a giant artificial atom in waveguide quantum electrodynamics, Phys. Rev. A **103**, 023710 (2021).

[33] A. Wallraff, D. I. Schuster, A. Blais, J. M. Gambetta, J. Schreier, L. Frunzio, M. H. Devoret, S. M. Girvin, and R. J. Schoelkopf, Sideband Transitions and Two-Tone Spectroscopy of a Superconducting Qubit Strongly Coupled to an On-Chip Cavity, Phys. Rev. Lett. **99**, 050501 (2007).

[34] B.-M. Ann and G. A. Steele, Tunable and weakly invasive probing of a superconducting resonator based on electromagnetically induced transparency, Phys. Rev. A **102**, 053721 (2020).

[35] K.-H. Chiang and Y.-F. Chen, Tunable Λ-type system made of a superconducting qubit pair, Phys. Rev. A **106**, 023707 (2022).

[36] P. M. Leung and B. C. Sanders, Coherent Control of Microwave Pulse Storage in Superconducting Circuits, Phys. Rev. Lett. **109**, 253603 (2012).

[37] J. D. Brehm, A. N. Poddubny, A. Stehli, T. Wolz, H. Rotzinger, and A. V. Ustinov, Waveguide bandgap engineering with an array of superconducting qubits, npj Quantum Mater. **6**, 10 (2021).

[38] J. D. Brehm, R. Gebauer, A. Stehli, A. N. Poddubny, O. Sander, H. Rotzinger, and A. V. Ustinov, Slowing down light in a qubit metamaterial, Appl. Phys. Lett. **121**, 204001 (2022).

[39] J. Koch, T. M. Yu, J. Gambetta, A. A. Houck, D. I. Schuster, J. Majer, A. Blais, M. H. Devoret, S. M. Girvin, and R. J. Schoelkopf, Charge-insensitive qubit design derived from the Cooper pair box, Phys. Rev. A **76**, 042319 (2007).

[40] A. Blais, J. Gambetta, A. Wallraff, D. I. Schuster, S. M. Girvin, M. H. Devoret, and R. J. Schoelkopf, Quantum-information processing with circuit quantum electrodynamics, Phys. Rev. A **75**, 032329 (2007).

[41] J. D. Strand, M. Ware, F. Beaudoin, T. A. Ohki, B. R. Johnson, A. Blais, and B. L. T. Plourde, First-order sideband transitions with flux-driven asymmetric transmon qubits, Phys. Rev. B **87**, 220505(R) (2013).

[42] N. Didier, E. A. Sete, M. P. da Silva, and C. Rigetti, Analytical modeling of parametrically modulated transmon qubits, Phys. Rev. A **97**, 022330 (2018).

[43] S. A. Caldwell, N. Didier, C. A. Ryan, E. A. Sete, A. Hudson, P. Karalekas, R. Manenti, M. P. da Silva, R. Sinclair, E. Acala *et al.*, Parametrically Activated Entangling Gates Using Transmon Qubits, Phys. Rev. Appl. **10**, 034050 (2018).

[44] X. Li, Y. Ma, J. Han, T. Chen, Y. Xu, W. Cai, H. Wang, Y. P. Song, Z.-Y. Xue, Z.-Q. Yin *et al.*, Perfect Quantum State Transfer in a Superconducting Qubit Chain with Parametrically Tunable Couplings, Phys. Rev. Appl. **10**, 054009 (2018).

[45] E. A. Sete, J. M. Martinis, and A. N. Korotkov, Quantum theory of a bandpass Purcell filter for qubit readout, Phys. Rev. A **92**, 012325 (2015).

[46] Q.-C. Liu, T.-F. Li, X.-Q. Luo, H. Zhao, W. Xiong, Y.-S. Zhang, Z. Chen, J. S. Liu, W. Chen, F. Nori *et al.*, Method for identifying electromagnetically induced transparency in a tunable circuit quantum electrodynamics system, Phys. Rev. A **93**, 053838 (2016).

[47] O. Astafiev, A. M. Zagoskin, A. A. Abdumalikov, Jr., Y. A. Pashkin, T. Yamamoto, K. Inomata, Y. Nakamura, and J. S. Tsai, Resonance fluorescence of a single artificial atom, Science **327**, 840 (2010).

[48] D. Roy, C. M. Wilson, and O. Firstenberg, *Colloquium*: Strongly interacting photons in one-dimensional continuum, Rev. Mod. Phys. **89**, 021001 (2017).

[49] A. S. Sheremet, M. I. Petrov, I. V. Iorsh, A. V. Poshakinskiy, and A. N. Poddubny, Waveguide quantum electrodynamics: Collective radiance and photon-photon correlations, Rev. Mod. Phys. **95**, 015002 (2023).

[50] A. A. Houck, D. I. Schuster, J. M. Gambetta, J. A. Schreier, B. R. Johnson, J. M. Chow, L. Frunzio, J. Majer, M. H. Devoret, S. M. Girvin, and R. J. Schoelkopf, Generating single microwave photons in a circuit, Nature (London) **449**, 328 (2007).

[51] J. Li, M. P. Silveri, K. S. Kumar, J.-M. Pirkkalainen, A. Vepsäläinen, W. C. Chien, J. Tuorila, M. A. Sillanpää, P. J. Hakonen, E. V. Thuneberg, and G. S. Paraoanu, Motional averaging in a superconducting qubit, Nat. Commun. **4**, 1420 (2013).

[52] J. P. Johansson, P. D. Nation, and F. Nori, QuTiP: An open-source Python framework for the dynamics of open quantum systems, Comput. Phys. Commun. **183**, 1760 (2012).

[53] K. Lalumière, B. C. Sanders, A. F. van Loo, A. Fedorov, A. Wallraff, and A. Blais, Input-output theory for waveguide QED with an ensemble of inhomogeneous atoms, Phys. Rev. A **88**, 043806 (2013).

[54] P. Anisimov and O. Kocharovskaya, Decaying-dressed-state analysis of a coherently driven three-level Λ system, J. Mod. Opt. **55**, 3159 (2008).

[55] X. Gu, A. F. Kockum, A. Miranowicz, Y.-X. Liu, and F. Nori, Microwave photonics with superconducting quantum circuits, Phys. Rep. **718–719**, 1 (2017).

[56] T. Y. Abi-Salloum, Electromagnetically induced transparency and Autler-Townes splitting: Two similar but distinct phenomena in two categories of three-level atomic systems, Phys. Rev. A **81**, 053836 (2010).

[57] X. Wang, H.-R. Li, D.-X. Chen, W.-X. Liu, and F.-l. Li, Tunable electromagnetically induced transparency in a composite superconducting system, Opt. Commun. **366**, 321 (2016).

[58] X. Wang, A. Miranowicz, H.-R. Li, F.-L. Li, and F. Nori, Two-color electromagnetically induced transparency via modulated coupling between a mechanical resonator and a qubit, Phys. Rev. A **98**, 023821 (2018).

[59] P. R. Rice and R. J. Brecha, Cavity induced transparency, Opt. Commun. **126**, 230 (1996).

[60] A. Blais, A. L. Grimsmo, S. M. Girvin, and A. Wallraff, Circuit quantum electrodynamics, Rev. Mod. Phys. **93**, 025005 (2021).

[61] C. W. Gardiner and M. J. Collett, Input and output in damped quantum systems: Quantum stochastic differential equations and the master equation, Phys. Rev. A **31**, 3761 (1985).

[62] M. J. Collett and C. W. Gardiner, Squeezing of intracavity and traveling-wave light fields produced in parametric amplification, Phys. Rev. A **30**, 1386 (1984).

[63] W.-J. Lin, Y. Lu, P. Y. Wen, Y.-T. Cheng, C.-P. Lee, K. T. Lin, K. H. Chiang, M. C. Hsieh, C.-Y. Chen, C.-H. Chien *et al.*, Deterministic loading of microwaves onto an artificial atom using a time-reversed waveform, Nano Lett. **22**, 8137 (2022).

[64] A. V. Gorshkov, A. André, M. Fleischhauer, A. S. Sørensen, and M. D. Lukin, Universal Approach to Optimal Photon Storage in Atomic Media, Phys. Rev. Lett. **98**, 123601 (2007).

[65] I. Novikova, A. V. Gorshkov, D. F. Phillips, A. S. Sørensen, M. D. Lukin, and R. L. Walsworth, Optimal Control of Light Pulse Storage and Retrieval, Phys. Rev. Lett. **98**, 243602 (2007).

[66] K. F. Reim, J. Nunn, V. O. Lorenz, B. J. Sussman, K. C. Lee, N. K. Langford, D. Jaksch, and I. A. Walmsley, Towards high-speed optical quantum memories, Nat. Photon. **4**, 218 (2010).

[67] E. Saglamyurek, T. Hrushevskyi, A. Rastogi, K. Heshami, and L. J. LeBlanc, Coherent storage and manipulation of broadband photons via dynamically controlled Autler–Townes splitting, Nat. Photon. **12**, 774 (2018).

[68] P. Alsing, D.-S. Guo, and H. J. Carmichael, Dynamic Stark effect for the Jaynes-Cummings system, Phys. Rev. A **45**, 5135 (1992).

Correction: The previously published Figure 1 contained an error and has been replaced.